Origin of and tuning the optical and fundamental band gaps in transparent conducting oxides: The case of $M_2O_3(M = \mathrm{Al, Ga, In})$

Fernando P. Sabino, Rafael Besse, and Luiz Nunes Oliveira
São Carlos Institute of Physics, University of São Paulo, P.O. Box 369, 13560-970, São Carlos, São Paulo, Brazil

Su-Huai Wei
Beijing Computational Science Research Center, Beijing 100094, China

Juarez L. F. Da Silva*
São Carlos Institute of Chemistry, University of São Paulo, P.O. Box 780, 13560-970, São Carlos, São Paulo, Brazil

(Received 29 June 2015; revised manuscript received 18 September 2015; published 23 November 2015)

Good transparent conducting oxides (TCOs), such as In_2O_3:Sn (ITO), usually combine large optical band gaps, essential for high transparency, with relatively small fundamental band gaps due to low conduction-band minima, which favor n-type doping and enhance the electrical conductivity. It has been understood that the optical band gaps are wider than the fundamental band gaps because optical transitions between the band-edge states are forbidden. The mechanism blocking such transitions, which can play a crucial role in the designing of alternative TCOs, nonetheless remains obscure. Here, based on first-principles density functional theory calculations and symmetry analysis of three oxides, M_2O_3 (M = Al, Ga, In), we identify the physical origin of the gap disparities. Three conditions are necessary: (1) the crystal structure must have global inversion symmetry; (2) in order to belong to the A_g or A_{1g} irreducible representations, the states at the conduction-band minimum must have cation and oxygen s character; (3) in order to have g parity, the oxygen p orbitals constituting the states near the valence-band maximum must be strongly coupled to the cation d orbitals. Under these conditions, optical excitations across the fundamental gap will be forbidden. The three criteria explain the trends in the M_2O_3 (M = Al, Ga, In) sequence, in particular, explaining why In_2O_3 in the bixbyite structure yields the highest figure of merit. Our study provides guidelines expected to be instrumental in the search for new TCO materials.

DOI: 10.1103/PhysRevB.92.205308 PACS number(s): 78.20.−e, 71.15.Mb, 71.20.−b, 74.25.Gz

I. INTRODUCTION

A wide range of such modern technological applications as solar cells [1], transparent transistors [2,3], light-emitting diodes [4], display panels [5], etc. require materials combining high transparency in the visible-spectrum range with high electrical conductivity. High optical transparencies are usually associated with wide band gaps (e.g., larger than 3 eV), while high electrical conductivity calls for elevated carrier densities (e.g., in the 10^{18} cm^{-3} to 10^{23} cm^{-3} range) [6]. Such concentrations being incompatible with large gaps, the transparency of tin-doped indium oxide (ITO) posed a longstanding puzzle.

For several decades now, ITO (In_2O_3:Sn) has been the material of choice for applications in optoelectronic devices [7] and also the prototype material in studies focused on raising the figure of merit of transparent conducting materials [7]. Only recently has it been understood that the outstanding properties of the doped oxide are due to the sizable difference (~ 0.8 eV) between its relatively small (2.9 eV) fundamental band gap and its large (3.7 eV) optical band gap [8]. The fundamental band gap is small because the large In cation in In_2O_3 lowers the antibonding state at the conduction-band minimum (CBM), which allows high n-type doping and yields high electron concentration [9]. The optical gap, which allows more than 80% transparency in the visible spectrum, is substantially wider because optical transitions between the valence-band maximum (VBM) and CBM states are forbidden [8].

The wide usage of transparent conduction oxides and the high cost of indium [5] has spurred the search for alternative transparent conducting oxides (TCOs). More profound understanding of the relation between the difference between the optical and fundamental band gaps, ΔE_g^{OF}, in TCOs and the structural and atomistic properties of the compounds and their constituents is, therefore, highly desirable. Can we control ΔE_g^{OF}? To address this question, we have selected a group of oxides, namely, M_2O_3 (M = Al, Ga, In), computed their equilibrium electronic structures employing density-functional theory (DFT), and analyzed their symmetries. For these materials, with centrosymmetric crystal structures and CBM chiefly constituted by cation and oxygen s states, our comparative analysis shows that the energy of the cationic d orbital controls the mismatch between the optical and fundamental gaps. To provide more evidence, we have added a Hubbard-model Coulomb repulsion to the 3d orbitals of Ga and to the 4d orbitals of In, which gave control over the d-level energies within the band structure [10] and over the coupling between the oxygen p orbitals and the cationic d orbitals. The results ratify our conclusion. The more strongly the p and d orbitals couple, the larger ΔE_g^{OF} will be.

II. THEORETICAL APPROACH AND COMPUTATIONAL DETAILS

Our DFT [11,12] calculations have adopted the semilocal Perdew-Burke-Ernzerhof (PBE) exchange-correlation

*juarez_dasilva@iqsc.usp.br

TABLE I. Equilibrium lattice parameters a_0, b_0, c_0, β, effective coordination numbers (ECNs) for the Al, Ga, and In atoms, and weighted-average bond lengths d_{av} separating the Al, Ga, and In atoms from the nearest O neighbor for all nonequivalent cation sites [19]. The bold numbers represent the ground-state structural parameters for the most stable structure of each oxide; for comparison, the row below each set displays the pertinent experimental parameters [20–22].

System	Structure	Space group	a_0 (Å)	b_0 (Å)	c_0 (Å)	β (degree)	ECN	d_{av} (Å)	Ref.
Al_2O_3	Corundum	$R\bar{3}c$	**4.81**		**13.11**		**5.82**	**1.92**	
	Corundum	$R\bar{3}c$	4.76		12.99		5.76	1.86	[22]
	Gallia	$C2/m$	11.92	2.94	5.67	103.96	3.99, 5.82	1.78, 1.93	
	Bixbyite	$Ia\bar{3}$	8.97				5.86, 6.00	1.93, 1.93	
Ga_2O_3	Corundum	$R\bar{3}c$	5.07		13.64		5.71	2.01	
	Gallia	$C2/m$	**12.45**	**3.09**	**5.88**	**103.71**	**3.99**, **5.81**	**1.87**, **2.02**	
	Gallia	$C2/m$	12.23	3.04	5.80	103.70	3.99, 5.81	1.84, 1.98	[20]
	Bixbyite	$Ia\bar{3}$	9.41				5.88, 6.00	2.02, 2.02	
In_2O_3	Corundum	$R\bar{3}c$	5.58		14.77		5.83	2.21	
	Gallia	$C2/m$	12.32	3.36	6.92	106.14	4.47, 5.71	2.14, 2.20	
	Bixbyite	$Ia\bar{3}$	**10.29**				**5.94**, **6.00**	**2.21**, **2.21**	
	Bixbyite	$Ia\bar{3}$	10.12				5.94, 6.00	2.17, 2.19	[21]

functional [13]. To shift the cation d orbital within the band structure and control the coupling between the cation d and oxygen p orbitals, we have employed the Hubbard model proposed by Dudarev *et al.* [14]. In Dudarev's rotationally invariant approach, only the difference $U_{\text{eff}} = U - J$, not the individual Coulomb (U) and exchange (J) interactions, is relevant. We have solved the Kohn-Sham equations on the basis of the all-electron projected augmented wave (PAW) approach [15,16], as implemented in the Vienna *Ab-initio* Simulation Package (VASP) [17,18], with the PAW projectors provided by VASP, namely, O ($2s^2 2p^4$), Al ($3s^2 3p^1$), Ga ($3d^{10} 4s^2 4p^1$), and In ($4d^{10} 5s^2 5p^1$). To determine the equilibrium volume, we have minimized the quantum mechanic stress tensor and atomic forces on every atom, with a plane-wave cutoff energy of 600 eV. A cutoff of 450 eV has proved sufficient to compute the optical properties, density of states, and band structures. To integrate over the Brillouin zone (BZ), we have used a $5\times5\times5$ k-point mesh (11 k-points in the irreducible part of the BZ) for the bixbyite structure and the same k-point density for the remaining systems.

III. RESULTS

A. Bulk crystal configuration

The Al_2O_3, Ga_2O_3, and In_2O_3 compounds crystallize in the corundum (rhombohedral, $R\bar{3}c$, $Z = 2$) [22], gallia (monoclinic, $C2/m$, $Z = 2$) [20], and bixbyite (body-centered cubic, $Ia\bar{3}$, $Z = 8$) structures, respectively, where Z denotes the number of formula units per primitive cell (see Supplemental Material [23]). Each corundum cation is surrounded by six oxygen atoms forming a distorted octahedral motif, while the bixbyite structure combines 25% ideal with 75% distorted octahedral. In contrast, the gallia structure combines 50% ideal tetrahedral with 50% distorted octahedral sites.

All three crystal structures are centrosymmetric, a property of capital importance in our analysis. Although Al, Ga, and In have the same valence and occupy the same column of the periodic table, the crystal structures of Al_2O_3, Ga_2O_3, and In_2O_3 are different, as mentioned above, because the cations have different sizes and because in the latter two compounds the O s orbitals hybridize with the Ga or In d orbitals, while the oxygen p orbitals are split from the cationic d orbitals [10]. For circumspection, we have computed the properties of the M_2O_3 compounds in the corundum, gallia, and bixbyite structures. For corundum Al_2O_3, gallia Ga_2O_3, and bixbyite In_2O_3, Table I shows that the equilibrium lattice parameters differ by less than 1.8% from the experimental values.

B. Band structure

Figure 1 displays the band structures for Al_2O_3, Ga_2O_3, and In_2O_3 in the corundum, gallia, and bixbyite structures, respectively. The highest valence bands in the ground states of the three M_2O_3 systems are nearly flat. In gallia Ga_2O_3, the VBM lies on the LM line (see Fig. S1, Supplemental Material [23]), only 0.03 eV above the Γ-point energy, while

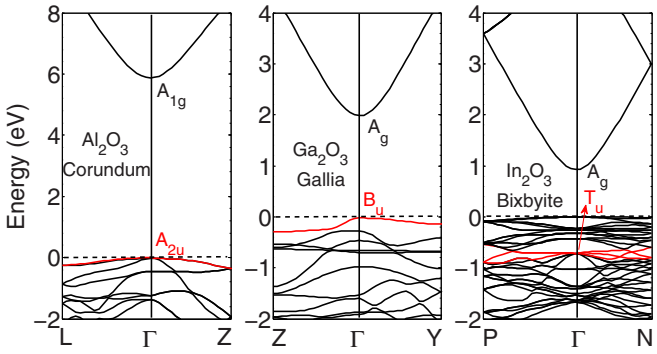

FIG. 1. (Color online) DFT-PBE band structure for Al_2O_3, Ga_2O_3, and In_2O_3 in the corundum, gallia, and bixbyite structures, respectively. The dashed lines indicate the valence-band maxima from which the energies are measured. The red solid lines identify the topmost states from which optical transitions to the conduction-band minima are allowed.

TABLE II. Calculated fundamental and optical band gaps for Al_2O_3, Ga_2O_3, and In_2O_3 in the corundum, gallia, and bixbyite structures. Indirect [direct] gaps are labeled (I) [(D)]. The differences ΔE_g^{OF} between the optical and fundamental band gaps at the Γ point are also shown. $\Delta E_g^{OF} > 0$ indicates that forbidden transitions make the fundamental gap narrower than the optical band gap. For the materials with indirect gaps, $\Delta E_g^{OF}(\Gamma)$ can be equal to zero even if $E_g^O > E_g^F$. For Ga_2O_3 and In_2O_3, ΔE_g^{OF} is also shown for two nonzero Hubbard-model U_{eff}'s: −10 eV and 10 eV.

System	Structure	U_{eff} (eV)	E_g^F (eV)	E_g^O (eV)	ΔE_g^{OF} (Γ) (eV)
Al_2O_3	Corundum	0	5.88 (D)	5.88	0.00
	Gallia	0	4.48 (I)	4.75	0.00
	Bixbyite	0	5.23 (I)	5.27	0.00
Ga_2O_3	Corundum	−10			0.00
		0	2.39 (I)	2.58	0.00
		10			0.00
	Gallia	−10			0.00
		0	1.98 (I)	2.01	0.00
		10			0.00
	Bixbyite	−10			0.96
		0	2.22 (I)	2.88	0.56
		10			0.39
In_2O_3	Corundum	−10			0.37
		0	0.95 (I)	1.19	0.16
		10			0.00
	Gallia	−10			0.00
		0	0.74 (I)	0.76	0.00
		10			0.00
	Bixbyite	−10			1.07
		0	0.93 (D)	1.64	0.71
		10			0.14

for corundum Al_2O_3 and bixbyite In_2O_3, the VBM occurs at the Γ point. The lowest conduction band is isotropic for all systems, with the CBM at the Γ point. In all cases, the second conduction-band state at the Γ point lies far above the CBM, a consequence of the strong ionic character of the systems under study that is prized in *n*-type TCOs because it impedes excitations within the conduction band. As expected, plain DFT-PBE underestimates the fundamental band gaps E_g^F. The theoretical (experimental) results for the M_2O_3 systems are 5.88 eV (9.25 eV [24]) for corundum Al_2O_3, 1.98 eV (4.90 eV [25]) for gallia Ga_2O_3, and 0.93 eV (2.90 eV [8]) for bixbyite In_2O_3.

We have also calculated the band structure for gallia and bixbyite Al_2O_3, corundum and bixbyite Ga_2O_3, and corundum and gallia In_2O_3. The results and the nature of the gaps are listed in Table II. The band structures are shown in Fig. S1 (Supplemental Material [23]). Although these crystal structures are less stable than those in Fig. 1, the electronic structures of the valence and conduction bands for each oxide are very similar to the corresponding bands in the figure, and even for those with indirect gaps the smallest direct gap is at the Γ point.

C. Density of states

Figure 2 shows the local densities of states (LDOS) for the three M_2O_3 systems and three structures under study. The ground-state structures occupy the main diagonal of the matrix formed by the nine panels. For all systems, the VBM and its vicinity are mainly constituted by O *p* states. While the conduction band mostly comprises cation *s* states and oxygen *p* states, the cation and oxygen *s* states are dominant at the CBM. Most of the contribution from the cation *d* states is concentrated in an energy range near −10 to −15 eV, the limits of which depend somewhat on the crystal structure and cationic species.

Within this range, the In 4*d* states are shallower than the Ga 3*d* states. For any of the three structures, the *d* states with M = In are always closer to the VBM than the *d* states with M = Ga. Among the three structures, gallia accommodates the deepest *d* states in M_2O_3 (M = Ga, In), because the tetrahedral environment enhances the coupling between the O *p*- and M *d*-states. The effect of the coupling is, however, less intense in In_2O_3, because the tetrahedra are distorted, as indicated by the (significantly larger than 4) effective coordination number (ECN) in Table I. The In *d* states are therefore closer to the VBM. The energy of the *d* orbitals and their coupling to the O *p* orbitals dictates the symmetry of the VBM states and hence controls the disparity between the fundamental and optical gaps, as discussed in Sec. III D.

D. Optical properties

To determine the optical band gap for the nine systems in our study, we have calculated the optical-transition matrix elements and analyzed the symmetries of the pertinent initial and final states. The optical band gap E_g^O is the smallest energy difference associated with valence-band–to–CBM transitions with large dipole matrix elements. Given that the transition matrix elements are continuous, analysis of a single point in reciprocal space suffices, and we have opted to compute the difference $\Delta E_g^{OF} = E_g^O - E_g^F$ between the optical and fundamental band gaps at the Γ point, on which we focus our discussion.

Table II shows that ΔE_g^{OF} depends on the crystal symmetry and cationic species. For Al_2O_3 in the corundum, gallia, and bixbyite structures, $\Delta E_g^{OF} = 0$. For Ga_2O_3, ΔE_g^{OF} also vanishes in the corundum and gallia structures, but $\Delta E_g^{OF} = 0.56$ eV in the bixbyite structure. For In_2O_3, in agreement with previous results by Walsh *et al.* [8], we have found that $\Delta E_g^{OF} = 0.71$ eV in the bixbyite structure. In the corundum and gallia structures, $\Delta E_g^{OF} = 0.16$ eV and $\Delta E_g^{OF} = 0$, respectively.

Symmetry considerations explain these results. Consider the electronic states in the vicinity of the VBM and CBM. The CBM is essentially constituted by cation and O *s* states belonging to the A_{1g} (corundum) or A_g (gallia and bixbyite) representations. Given the sizable splitting between the CBM and the second conduction band at the Γ point, we only have to consider transitions to the CBM, which is even (g) under inversion. Consequently, since the dipole moment is odd under inversion, only transitions from states belonging to odd (u) representations are allowed. In the corundum structure, the allowed (i.e., odd) initial states belong to the A_{2u} and E_u representations. In the gallia structure, the allowed states belong to the A_u and B_u representations, and in the

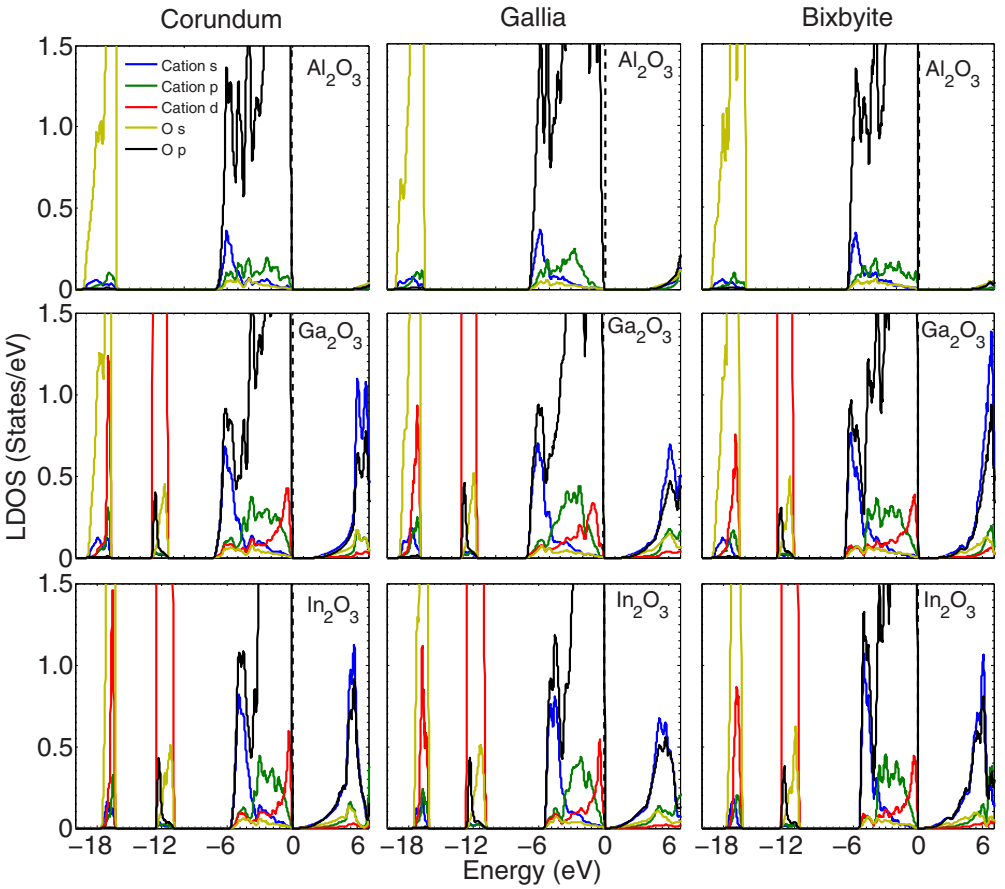

FIG. 2. (Color online) Local density of states for Al_2O_3, Ga_2O_3, and In_2O_3 in the corundum, gallia, and bixbyite structures. In each panel, the valence-band maximum (conduction-band minimum) is mainly composed by O p states (cation and oxygen s states). In each crystal structure, compared with the In 4d level in In_2O_3, the Ga 3d level in Ga_2O_3 lies deeper in the valence band.

bixbyite structure, to the T_u representation. The most energetic valence-band states with significant dipole matrix elements with the CBM are highlighted in Fig. 1. For the nine systems under study, Table III lists the symmetry representations of the topmost few valence states at the Γ point, distinguishes the allowed transitions from the forbidden ones, and presents the computed transition amplitudes, in arbitrary units.

Table III shows how the fundamental and optical gaps depend on the metallic species. In the corundum structure, the topmost and second valence bands in Al_2O_3 belong to the A_{2u} and E_u representations and hence allow transitions to the CBM. If the cation is Ga instead of Al, the topmost and second valence bands are still odd, E_u and A_{2u}, respectively, but the third state, of the E_g representation, is only 0.09 eV below the VBM. In In_2O_3, the E_g state lies 0.16 eV above the E_u state, which in turn is above the A_{2u} level. Transitions being forbidden between the E_g band and the CBM, it follows that the gap difference in corundum In_2O_3 is $\Delta E_g^{\mathrm{OF}} = 0.16$ eV. Briefly stated, the In d orbitals push the E_g state to the top of the valence band and make $\Delta E_g^{\mathrm{OF}} > 0$ in corundum In_2O_3. By contrast, the energies of the Ga 3d states in Ga_2O_3 being considerably more negative than the energies of the In 4d orbitals in In_2O_3, the coupling between the Ga d orbitals and the O p orbitals is not strong enough to push the E_g to the VBM, so that $\Delta E_g^{\mathrm{OF}} = 0$ in corundum Ga_2O_3.

In the gallia structure, due to the tetrahedral environment of half of the cations, the VBM belongs to the B_u representation, independently of the cation. Consequently, $\Delta E_g^{\mathrm{OF}} = 0$ for gallia M_2O_3 (M = Al, Ga, In). The higher ECN in gallia In_2O_3 raises the energy of the A_g and B_g states, from which transitions to the CBM are forbidden. Still, as Table III shows, the two even states lie below the B_u VBM state, from which transitions to the CBM are allowed, so that $\Delta E_g^{\mathrm{OF}} = 0$. Along the M_2O_3 sequence, the progressively stronger p-d coupling in the tetrahedral environment makes the band structure more direct, i.e., reduces the energy difference between the VBM at the Γ point and the highest occupied molecular orbital (HOMO) from 0.27 eV (Al_2O_3), to 0.03 eV (Ga_2O_3), and 0.02 eV (In_2O_3).

In the bixbyite structure, the gap differences follow the pattern set by the corundum symmetry. ΔE_g^{OF} grows from 0 in Al_2O_3, to 0.56 eV in Ga_2O_3, to 0.71 eV in In_2O_3, as the cation d orbitals couple more strongly to the oxygen p orbitals. Our computation of ΔE_g^{OF} has disregarded a few allowed transitions from fold-in states in Ga_2O_3 and In_2O_3, resultant from the large bixbyite unit cell, whose amplitudes are less than 23.1% and 2.8%, respectively, of the transition at the Γ point. These transitions, along with others from k points close to the Γ point, account for the small shoulder in the absorption spectrum reported in the experimental study of

TABLE III. Irreducible representations of the conduction-band minima and valence-band states involved in optical transitions. All states are at the Γ point. Energies are measured from the valence-band maximum, so that positive (negative) energies indicate states in the conduction (valence) band. Each occupation and transition amplitude corresponds to a single band.

System	Structure	Band	Energy (eV)	Occupation	Symmetry	Transition	Type transition	Amplitude (a.u.)
Al_2O_3	Corundum	25	5.88	0.00	A_{1g}			
		24	0.00	2.00	A_{2u}	$A_{2u} \rightarrow A_{1g}$	Allowed	8.85
		22, 23	−0.03	2.00	E_u	$E_u \rightarrow A_{1g}$	Allowed	8.40
		20, 21	−0.46	2.00	E_g	$E_g \rightarrow A_{1g}$	Forbidden	0.00
		18, 19	−1.24	2.00	E_g	$E_g \rightarrow A_{1g}$	Forbidden	0.00
Al_2O_3	Gallia	25	4.75	0.00	A_g			
		24	0.00	2.00	B_u	$B_u \rightarrow A_g$	Allowed	7.58
		23	−0.24	2.00	B_u	$B_u \rightarrow A_g$	Allowed	8.17
		22	−0.32	2.00	A_g	$A_g \rightarrow A_g$	Forbidden	0.00
		21	−0.71	2.00	A_u	$A_u \rightarrow A_g$	Allowed	7.96
Al_2O_3	Bixbyite	97	1.33	0.00	A_g			
		94, 95, 96	0.00	2.00	T_u	$T_u \rightarrow A_g$	Allowed	1.67
		91, 92, 93	−0.33	2.00	T_g	$T_g \rightarrow A_g$	Forbidden	0.00
		88, 89, 90	−0.36	2.00	T_u	$T_u \rightarrow A_g$	Allowed	0.14
		87	−0.40	2.00	A_g	$A_g \rightarrow A_g$	Forbidden	0.00
Ga_2O_3	Corundum	45	2.58	0.00	A_{1g}			
		43, 44	0.00	2.00	E_u	$E_u \rightarrow A_{1g}$	Allowed	18.61
		42	−0.07	2.00	A_{2u}	$A_{2u} \rightarrow A_{1g}$	Allowed	34.81
		40, 41	−0.09	2.00	E_g	$E_g \rightarrow A_{1g}$	Forbidden	0.00
		38, 39	−0.28	2.00	E_g	$E_g \rightarrow A_{1g}$	Forbidden	0.00
Ga_2O_3	Gallia	45	2.01	0.00	A_g			
		44	0.00	2.00	B_u	$B_u \rightarrow A_g$	Allowed	28.61
		43	−0.26	2.00	B_u	$B_u \rightarrow A_g$	Allowed	28.07
		42	−0.44	2.00	A_g	$A_g \rightarrow A_g$	Forbidden	0.00
		41	−0.64	2.00	A_u	$A_u \rightarrow A_g$	Allowed	5.76
Ga_2O_3	Bixbyite	177	2.32	0.00	A_g			
		174, 175, 176	0.00	2.00	T_g	$T_g \rightarrow A_g$	Forbidden	0.00
		171, 172, 173	−0.19	2.00	T_u	$T_u \rightarrow A_g$	Allowed	0.20
		170	−0.19	2.00	A_g	$A_g \rightarrow A_g$	Forbidden	0.00
		168, 169	−0.25	2.00	E_g	$E_g \rightarrow A_g$	Forbidden	0.00
		165, 166, 167	−0.35	2.00	T_u	$T_u \rightarrow A_g$	Allowed	1.35
		162, 163, 164	−0.35	2.00	T_g	$T_g \rightarrow A_g$	Forbidden	0.00
		159, 160, 161	−0.56	2.00	T_u	$T_u \rightarrow A_g$	Allowed	5.84
		156, 157, 158	−0.87	2.00	T_g	$T_g \rightarrow A_g$	Forbidden	0.00
In_2O_3	Corundum	45	1.03	0.00	A_{1g}			
		43, 44	0.00	2.00	E_g	$E_g \rightarrow A_{1g}$	Forbidden	0.00
		41, 42	−0.16	2.00	E_u	$E_u \rightarrow A_{1g}$	Allowed	20.25
		39, 40	−0.27	2.00	E_g	$E_g \rightarrow A_{1g}$	Forbidden	0.00
		38	−0.38	2.00	A_{2u}	$A_{2u} \rightarrow A_{1g}$	Allowed	77.08
In_2O_3	Gallia	45	0.76	0.00	A_g			
		44	0.00	2.00	B_u	$B_u \rightarrow A_g$	Allowed	118.00
		43	−0.16	2.00	A_g	$A_g \rightarrow A_g$	Forbidden	0.00
		42	−0.35	2.00	B_g	$B_g \rightarrow A_g$	Forbidden	0.00
		41	−0.42	2.00	A_u	$A_u \rightarrow A_g$	Allowed	9.68
In_2O_3	Bixbyite	177	0.93	0.00	A_g			
		174, 175, 176	0.00	2.00	T_g	$T_g \rightarrow A_g$	Forbidden	0.00
		171, 172, 173	−0.22	2.00	T_u	$T_u \rightarrow A_g$	Allowed	0.37
		170	−0.23	2.00	A_g	$A_g \rightarrow A_g$	Forbidden	0.00
		168, 169	−0.26	2.00	E_g	$E_g \rightarrow A_g$	Forbidden	0.00
		165, 166, 167	−0.32	2.00	T_g	$T_g \rightarrow A_g$	Forbidden	0.00
		162, 163, 164	−0.42	2.00	T_u	$T_u \rightarrow A_g$	Allowed	0.25
		159, 160, 161	−0.71	2.00	T_u	$T_u \rightarrow A_g$	Allowed	13.12
		156, 157, 158	−0.72	2.00	T_g	$T_g \rightarrow A_g$	Forbidden	0.00

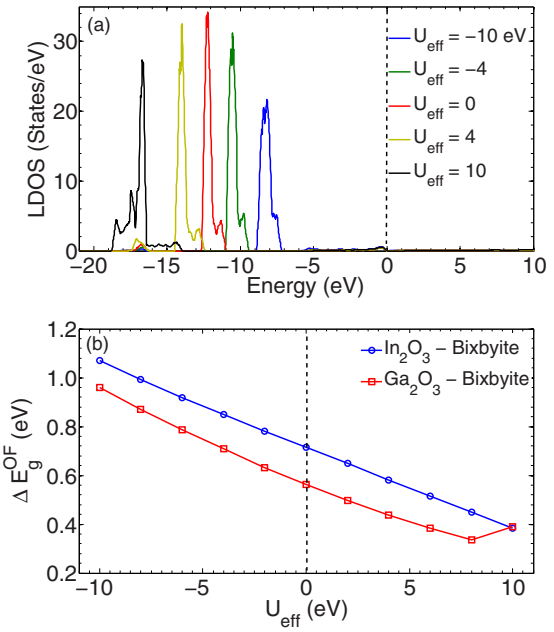

FIG. 3. (Color online) (a) Local density of states for In d orbital in the bixbyite structure for the indicated effective Coulomb repulsions U_{eff}. (b) Difference between the optical and fundamental band gaps in bixbyite In_2O_3 and Ga_2O_3 as a function of U_{eff}. The open squares and circles represent the differences between the optical gap, defined by the $T_u \rightarrow A_g$ transition and the fundamental gaps in bixbyite Ga_2O_3 and In_2O_3, respectively, where the final state A_g is at the conduction-band minimum, and T_u is the triply degenerate state belonging to bands 165–167 (Ga_2O_3) or 159–161 (In_2O_3) in Table III. For clarity, we have computed the optical gap from the same initial and final states throughout the range $-10\,\text{eV} \leqslant U_{\text{eff}} \leqslant 10\,\text{eV}$, even though the transitions from the T_u states in the 171–173 band (for Ga_2O_3) and the 162–164 band (for In_2O_3) to the A_g state in the interval $6\,\text{eV} < U_{\text{eff}} \leqslant 10\,\text{eV}$ have larger amplitude than the reference transitions. The blue solid line through the open circles and the red solid line through the open squares are guides to the eye.

bixbyite In_2O_3 [8]. If bixbyite Ga_2O_3 were available in the laboratory, a significantly more pronounced shoulder would be observed. In any case, the transitions responsible for the shoulders are too weak to narrow the optical gap.

E. Tuning the optical band gap

To demonstrate that the p-d coupling controls the disparity between the optical and fundamental band gaps, we have used the Hubbard model to shift the cation d-state energy. By setting the energy of the d states, the Hubbard U_{eff} determines the strength of the p-d hybridization and the position of the resulting bands. As an example, Fig. 3(a) depicts the density of states for the In $4d$ orbitals in bixbyite In_2O_3, with U_{eff} ranging from -10 to 10 eV. As U_{eff} grows in that range, the evolution of the density of states shows that the d states move down in energy, away from the O p states in the vicinity of the VBM. The p-d coupling is progressively weakened.

Figure 3(b) shows ΔE_g^{OF} as a function of U_{eff} for bixbyite Ga_2O_3 and In_2O_3, the two systems for which ΔE_g^{OF} varies most widely. Consider first the open circles, which depict the energy differences for In_2O_3, computed from the optical gap defined by the transition from the (triply degenerate) T_u states in the 159–161 bands in Table III. For $U_{\text{eff}} = -10$ eV, as Table II shows, the energy difference is $\Delta E_g^{\text{OF}} = 1.07$ eV, positive because the T_g states at the VBM lie 1.07 eV above the T_u states defining the optical gap. Increasing U_{eff} is analogous to substituting M = Ga, and then M = Al, for M = In in M_2O_3 . As U_{eff} grows, therefore, the hybridization between the O p states and the In d states weakens, the T_g states are pushed down in energy, and the fundamental gap widens. The disparity between the optical and fundamental gaps therefore diminishes, from $\Delta E_g^{\text{OF}} = 1.07$ eV at $U_{\text{eff}} = -10$ eV to $\Delta E_g^{\text{OF}} = 0.14$ eV at $U_{\text{eff}} = 10$ eV.

Likewise, for bixbyite Ga_2O_3, represented by red open squares in the figure, the optical gap is defined by the transition from the T_u states in the 165–167 band in Table III to the A_g state at the CBM. Since these T_u states lie 0.96 eV below the T_g state at the VBM, the optical gap is substantially wider than the fundamental gap. As U_{eff} grows, the hybridization between the O p orbitals and the Ga d orbitals weakens, and the T_g state at the VBM is displaced downward in energy. E_g^F therefore grows, and ΔE_g^{OF} shrinks. For sufficiently large effective Coulomb repulsion, at $U_{\text{eff}} = 8$ eV, the T_g states sink below the T_u states belonging to the 171–173 band in Table III. Since these T_u states, which now lie at the VBM, continue to rise in energy as U_{eff} grows, ΔE_g^{OF} grows in the interval $8\,\text{eV} \leqslant U_{\text{eff}} \leqslant 10\,\text{eV}$.

The steep slopes of the two plots in Fig. 3(b) show that the coupling between the cationic d orbitals and the O p orbitals controls the gap disparity. More generally, in TCOs with (i) inversion symmetry and (ii) CBM belonging to the A_g or A_{1g} representations, the p-d hybridization tunes the forbidden-transition energy. Likewise, in systems with strong valence-band s-p coupling, we expect the splitting of orbital parities to enhance the disparity between the optical and fundamental band gaps. Our finding pinpoints the requirements for a sizable gap disparity and hence adds predictive power to the search for new transparent conductors. Moreover, it allows tuning of the optical band gap to higher figures of merit. For example, the substitution of In for Ga atoms in the bixbyite structure, or the substitution of In for Al atoms in the corundum structure, will enhance the gap disparity.

IV. CONCLUSION

In summary, we have studied the disparity between the optical and fundamental band gaps in the corundum, gallia, and bixbyite structures of the M_2O_3 (M = Al, Ga, In) oxides. We have shown that large ΔE_g^{OF} require the following conditions: (1) crystal structure with global and local inversion symmetries; (2) CBM comprising cation and O s states, so it belongs to the A_g or A_{1g} representations; and (3) strong coupling between d and p orbitals in states near the VBM. These conditions are satisfied in bixbyite In_2O_3, which explains the large difference between its optical and fundamental band gaps. In corundum Al_2O_3 and gallia Ga_2O_3, the optical and fundamental gaps are congruent because the third condition is violated. The insight derived from these requirements provides guidelines for designing TCOs with elevated figures of merit.

ACKNOWLEDGMENTS

This research was supported by the CNPq (Grants No. 403142/2012-1 and No. 409921/2013-0), CAPES, and FAPESP (Grant No. 2013/21045-2). The infrastructure provided to our computer cluster by the São Carlos Center of Informatics, University of São Paulo, is gratefully acknowledged.

[1] C. G. Granqvist, Sol. Energy Mater. Sol. Cells **91**, 1529 (2007).
[2] K. Nomura, H. Ohta, K. Ueda, T. Kamiya, M. Hirano, and H. Hosono, Science **300**, 1269 (2003).
[3] K. Nomura, H. Ohta, A. Takagi, T. Kamiya, M. Hirano, and H. Hosono, Nature (London) **432**, 488 (2004).
[4] J. J. Berry, D. S. Ginley, and P. E. Burrows, Appl. Phys. Lett. **92**, 193304 (2008).
[5] B. G. Lewis and D. C. Paine, MRS Bull. **25**, 22 (2000).
[6] K. Utsumi, O. Matsunaga, and T. Takahata, Thin Solid Films **334**, 30 (1998).
[7] I. Hamberg and C. G. Granqvist, J. Appl. Phys. **60**, R123 (1986).
[8] A. Walsh, J. L. F. Da Silva, S.-H. Wei, C. Korber, A. Klein, L. F. J. Piper, A. DeMasi, K. E. Smith, G. Panaccione, P. Torelli, D. J. Payne, A. Bourlange, and R. G. Egdell, Phys. Rev. Lett. **100**, 167402 (2008).
[9] A. Walsh, J. L. F. Da Silva, and S.-H. Wei, J. Phys.: Condens. Matter **23**, 334210 (2011).
[10] F. P. Sabino, L. N. de Oliveira, and J. L. F. Da Silva, Phys. Rev. B **90**, 155206 (2014).
[11] P. Hohenberg and W. Kohn, Phys. Rev. **136**, B864 (1964).
[12] W. Kohn and L. J. Sham, Phys. Rev. **140**, A1133 (1965).
[13] J. P. Perdew, K. Burke, and M. Ernzerhof, Phys. Rev. Lett. **77**, 3865 (1996).
[14] S. L. Dudarev, G. A. Botton, S. Y. Savrasov, C. J. Humphreys, and A. P. Sutton, Phys. Rev. B **57**, 1505 (1998).
[15] P. E. Blöchl, Phys. Rev. B **50**, 17953 (1994).
[16] G. Kresse and D. Joubert, Phys. Rev. B **59**, 1758 (1999).
[17] G. Kresse and J. Hafner, Phys. Rev. B **48**, 13115 (1993).
[18] G. Kresse and J. Furthmüller, Phys. Rev. B **54**, 11169 (1996).
[19] J. L. F. Da Silva, J. Appl. Phys. **109**, 023502 (2011).
[20] S. Geller, J. Chem. Phys. **33**, 676 (1960).
[21] M. Marezio, Acta Cryst. **20**, 723 (1966).
[22] P. Thompson, D. E. Cox, and J. B. Hastings, J. Appl. Cryst. **20**, 79 (1987).
[23] See Supplemental Material at http://link.aps.org/supplemental/10.1103/PhysRevB.92.205308 for the corundum, gallia and bixbyite crystal structures calculated for Al_2O_3, Ga_2O_3, and In_2O_3. Furthermore, we reported also the band structures for the three compounds calculated with the corundum, gallia, and bixbyite structures.
[24] T. Tomiki, Y. Ganaha, T. Shikenbaru, T. Futemma, M. Yuri, Y. Aiura, S. Sato, H. Fukutani, H. Kato, T. Miyahara, A. Yonesu, and J. Tamashiro, J. Phys. Soc. Jpn. **62**, 573 (1993).
[25] M. Orita, H. Ohta, M. Hirano, and H. Hosono, Appl. Phys. Lett. **77**, 4166 (2000).